Trapping a Single Vortex and Reducing Quasiparticles in a Superconducting Resonator

I. Nsanzineza and B. L. T. Plourde*
Department of Physics, Syracuse University, Syracuse, New York 13244-1130, USA
(Received 21 April 2014; revised manuscript received 14 July 2014; published 12 September 2014)

Vortices trapped in thin-film superconducting microwave resonators can have a significant influence on the resonator performance. Using a variable-linewidth geometry for a weakly coupled resonator, we are able to observe the effects of a single vortex trapped in the resonator through field cooling. For resonant modes where the vortex is near a current antinode, the presence of even a single vortex leads to a measurable decrease in the quality factor and a dispersive shift of the resonant frequency. For modes with the vortex located at a current node, the presence of the vortex results in no detectable excess loss and, in fact, produces an increase in the quality factor. We attribute this enhancement to a reduction in the density of nonequilibrium quasiparticles in the resonator due to their trapping and relaxation near the vortex core.

DOI: 10.1103/PhysRevLett.113.117002 PACS numbers: 84.40.Dc, 03.67.Lx, 74.25.Uv

Superconducting thin-film microwave resonators play a critical role in many areas including circuits for quantum information processing [1,2] and photon detectors for astrophysical applications [3]. Frequently, these resonators are operated in environments with a non-negligible magnetic field, perhaps due to insufficient magnetic shielding, magnetism in packaging and connector hardware, or pulsed magnetic fields for controlling circuit parameters.

The response of magnetic flux vortices in such resonators has been studied through field-cooled measurements and related to the vortex viscosity and pinning strength in different superconducting films [4]. In general, trapped vortices were found to cause a reduction in the resonator quality factor, with the magnitude of the effect scaling with the number of vortices, as well as a downwards shift in the resonance frequency. Patterned surface pinning [5] and other vortex-trapping structures [6,7] have been investigated for minimizing the excess loss contributions from vortices for circuits that require operation in large magnetic fields. These previous experiments have all involved resonators with many trapped vortices. The response of a single vortex in such a microwave circuit has not yet been explored.

In this Letter, we present field-cooled measurements of a coplanar-waveguide resonator with a geometry designed to allow vortex trapping in only a small region over a wide range of magnetic fields. Because the resonator is weakly coupled to the external circuitry and has a reasonably high internal quality factor Q_i, we are able to resolve the influence of individual vortices. In addition, we observe a dramatic difference in the effects of the first several trapped vortices on the particular resonance mode that we excite. When the vortices are near an antinode of the current standing-wave pattern, there is a stepwise increase in the loss. However, vortices located near a current node contribute no extra loss and, in fact, lead to a decrease in the loss, a process that we attribute to enhanced trapping of nonequilibrium quasiparticles due to the cores of the trapped vortices.

In order to control the location of the trapped vortices upon field cooling, we design our resonator to make use of the width dependence of the threshold perpendicular magnetic field for vortex trapping, B_{th}. For a trace of width w, $B_{\mathrm{th}}(w) \sim w^{-2}$, although there is also a logarithmic correction related to the vortex core energy that can be significant [8,9]. This relationship has been studied through vortex imaging experiments on superconducting strips of different widths cooled in a range of fields [10], and we have included an analysis of $B_{\mathrm{th}}(w)$ for our device in the Supplemental Material [11]. Thus, a wide trace will begin trapping vortices at a smaller field as compared to a narrow trace. Therefore, we design the center conductor of our coplanar-waveguide resonator to be 3 μm wide over most of its length, with a bulge having a width of 8 μm for the central 50 μm along the length of the resonator (Fig. 1). Furthermore, the ground plane contains an array of holes that are 5.6 μm wide and separated by a superconducting web with a linewidth of 2.8 μm to avoid the trapping of vortices outside of the central bulge region of the center conductor for fields below B_{th} for all of the narrower traces on the device.

Our resonator is 17.1 mm long and has an elbow-style capacitive coupler to a feed line at one end and an open circuit on the other end. The fundamental resonance corresponds to a half wavelength with a current antinode at the central bulge. The resonator is patterned from a 60-nm-thick Al film on a high-resistivity Si wafer using photolithography followed by a wet-etch process.

We cool the device on an adiabatic demagnetization refrigerator (ADR) with a 3 K pulse-tube cooled stage. The resonator chip is mounted on the cold finger of the ADR and is located at the center of a superconducting Helmholtz coil at 3 K. We repeatedly heat the cold finger to ~1.5 K to exceed T_c for the Al film and then cool to 100 mK while

 © 2014 American Physical Society

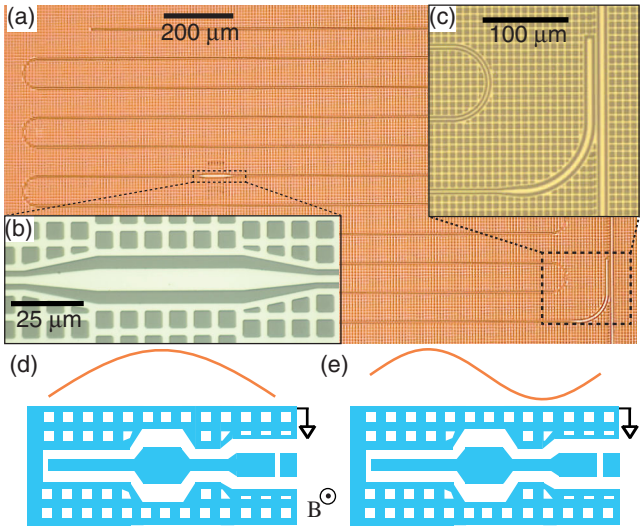

FIG. 1 (color online). Optical micrographs of (a) the entire resonator including feed line, (b) close-up of the bulge region for vortex trapping near the center of resonator, and (c) close-up of coupling elbow and feed line. Schematic of the resonator without turns (not to scale) along with a standing-wave pattern of microwave current for (d) fundamental and (e) first-harmonic resonance.

applying different magnetic fields with the Helmholtz coil. A cryogenic mu-metal can at 3 K shields the resonator from stray magnetic fields outside of the cryostat as well as any residual stray fields from the ADR magnet. By cooling in positive and negative magnetic fields applied from the Helmholtz coil and comparing any small asymmetry between measurements of the same vortex-trapping features (not shown), we estimate the component of the background magnetic field perpendicular to our sample to be less than 2 μT.

Upon reaching 100 mK for each field-cooling point, we measure the microwave transmission S_{21} through the feed line with a vector network analyzer. Following the subtraction of a separate calibration of the magnitude and phase of the background transmission, for each cooling field we fit S_{21}^{-1} in the complex plane with a four-parameter model [12] to extract the total quality factor Q for each cooling field. We measure S_{21} at sufficiently high powers ($\sim 10^5$ photons) in order to minimize the loss due to two-level defects on the surfaces and interfaces [13].

We observe the fundamental resonance at 3.0713 GHz with a coupling quality factor $Q_c = 765\,000$. For zero-field cooled measurements, we measure $Q = 185\,000$; thus, the resonator is significantly undercoupled with internal losses dominating coupling losses $(1/Q = 1/Q_i + 1/Q_c)$. At each cooling field, we extract the loss due to vortices by computing $1/Q_v = 1/Q(B) - 1/Q(B = 0)$ [4], thus subtracting out contributions from all other loss mechanisms, such as coupling to external circuitry or dielectric loss. For sufficiently small B, we observe $1/Q_v = 0$ as there are no

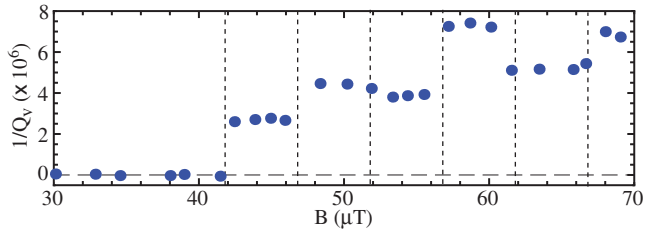

FIG. 2 (color online). $1/Q_v(B)$ for fundamental resonance for cooling fields in the vicinity of $B_{\text{th}}(8\ \mu\text{m})$ for the central bulge region. Vertical dashed lines correspond to field steps $\Delta B = 5\ \mu$T.

vortices trapped in the resonator (Fig. 2). At a cooling field of 42 μT, there is an abrupt step upwards in $1/Q_v$, which we attribute to the trapping of one vortex in the central bulge.

The first step in $1/Q_v$ is followed by a series of steps that are spaced by $\Delta B \approx 5\ \mu$T. Assuming each step corresponds to an increase in the number of vortices by one, this corresponds to an effective area for vortex trapping of $\Phi_0/\Delta B \approx 400\ \mu\text{m}^2$, which matches the area of the bulge region in our resonator, where $\Phi_0 \equiv h/2e$ is the magnetic flux quantum. While the step widths are quantized, as one would expect for the sequential addition of one vortex, the step heights are clearly not constant and, in fact, do not always have the same sign, as in the step from four to five vortices. Because $1/Q_v$ depends on the local current density, which will be highly nonuniform across the width of the bulge [4], vortices located near the edge of the bulge will contribute more loss compared to a vortex near the center line. The vortex positions are determined by the random pinning potential in the Al film as well as the intervortex interactions that are present immediately below T_c when the vortices are still mobile, before the vortices become pinned somewhat further below T_c [14]. At our measurement temperature, the superconducting penetration depth is less than 100 nm, and the vortices no longer interact with one another. Despite the variations in step height for our measurements, we can estimate an approximate loss per vortex by using Eq. (12) from Ref. [4] with parameters for the Al film on this device. We obtain a value between 1 and 5×10^{-6} depending on the vortex location with respect to the current density distribution, consistent with our measured steps in $1/Q_v$.

In addition to the fundamental, we can also measure the first harmonic at 6.1351 GHz, with $Q_c = 341\,000$, corresponding to a full-wavelength resonance with a current node at the central bulge. Thus, we expect that vortices trapped in the bulge should contribute no loss to this harmonic resonance, as there is no current present to drive the vortices. However, our measurements of $1/Q_v$ for the harmonic exhibit a *decrease* to lower loss at the same $B_{\text{th}}(8\ \mu\text{m})$ where we observe the first step upwards in $1/Q_v$ for the fundamental (Fig. 3). While this downwards trend

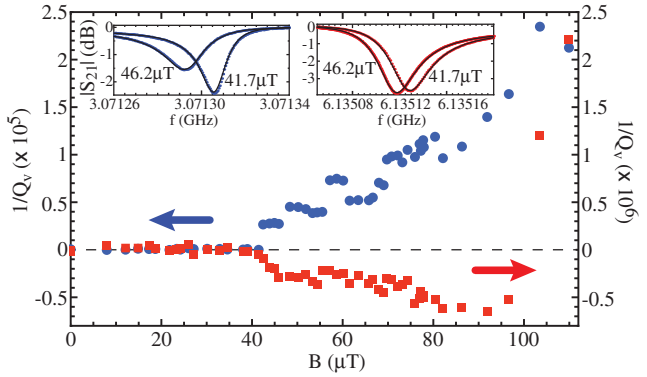

FIG. 3 (color online). $1/Q_v(B)$ for fundamental (blue circles) and first harmonic (red squares) resonance—note different scales on loss axes. (Insets) $|S_{21}(f)|$ for (left) fundamental and (right) harmonic for $B = 41.7$ (no vortices) and 46.2 μT (one-vortex step).

for the harmonic is clearly visible, it is not as sharp as the upwards step for the fundamental. Because the changes in $1/Q_v$ for the harmonic are about one order of magnitude weaker than those on the fundamental, slight variations in the extracted loss, due perhaps to variations in the temperature of our cryostat or changes in the electromagnetic environment for measuring the resonator from run to run, tend to smooth out small features in $1/Q_v(B)$ for the harmonic. $1/Q_v$ continues to decrease for larger cooling fields until a field of $\sim$90 μT, at which point there is a significant increase to higher loss values. We attribute this increase at large fields to vortices that begin to trap along the entire length of the resonator for $B > B_{\text{th}}(3\ \mu\text{m})$, where there are significant microwave currents to drive the vortices. For $B > 110$ μT, the internal losses from the vortices become large enough relative to the coupling loss $1/Q_c$ that we are unable to fit the resonance and extract a value for Q. We have chosen to focus our analysis on the changes in loss for the fundamental and harmonic rather than the shifts in the resonance frequencies. Because the resonator in this experiment is quite narrow over most of its length and thus has a substantial kinetic inductance contribution, nonlinear effects of the superconductor itself dominate the frequency response to changes in the magnetic field, as has been studied previously [15].

We interpret the decrease in $1/Q_v$ for the harmonic resonance in terms of a reduction in the loss due to quasiparticles $1/Q_{\text{qp}}$ due to interactions between quasiparticles and vortex cores. At our measurement temperature of 100 mK, the density of thermal quasiparticles should be vanishingly small. However, several recent investigations have demonstrated that, without extensive shielding of stray light, superconducting Al circuits measured at millikelvin temperatures can exhibit a significant excess of nonequilibrium quasiparticles with a typical volume density $n_{\text{qp}} \sim 10$–100 μm^{-3} [16–18]. Blackbody photons emitted by warmer regions of the measurement cryostat, even if only at a few Kelvin, can be sufficiently energetic to break Cooper pairs in Al films due to the relatively small superconducting energy gap. $1/Q_{\text{qp}}$ is proportional to the density of quasiparticles in the superconductor n_{qp}; thus, this mechanism can lead to excess loss [19].

Measurements of the effectiveness of different levels of infrared shielding of Al resonators were reported in Ref. [16], where the cryostat temperature on an ADR was increased while the cold finger was maintained below 150 mK. With minimal shielding, comparable to our setup, the high-power resonator loss was observed to increase with cryostat temperature, as one would expect for a blackbody source. We have performed the same measurement on our ADR with an identical resonator to the one presented here after zero-field cooling and observed a similar increase in loss with cryostat temperature (Supplemental Material [11]). Thus, we conclude that nonequilibrium quasiparticles also limit the loss of our resonators at the high power of our measurements. Following the analysis and Eq. (1) in Ref. [16] and using a kinetic inductance fraction of 0.27 that we measured on the same cooldown, we obtain $n_{\text{qp}} = 50$ μm^{-3} in zero field.

Interactions between quasiparticles and vortices have been studied previously in quasiparticle lifetime experiments [20] and also in the context of tunnel junction photon detectors [21] and normal metal-insulator-superconductor coolers [22]. These all involve many vortices trapped in the superconducting region with the suppressed gap in the vicinity of each vortex core providing a pathway for quasiparticle relaxation and trapping. In Ref. [20], quasiparticles were injected with a tunnel junction at one end of an Al strip, and their diffusion along the strip was measured with a second tunnel junction some distance away. The quasiparticle flux reaching the detector junction was significantly reduced when a magnetic field was used to generate vortices in the Al strip. This process was modeled with a quasiparticle diffusion equation with an extra recombination term depending on the fraction of nonsuperconducting regions, related to the density of vortices in the film.

We follow a related approach to model quasiparticle diffusion in our resonator but with discrete regions of enhanced recombination localized around each vortex. We treat the diffusion process in 1D, neglecting variations in the width of the center conductor of the resonator:

$$D\nabla^2 n_{\text{qp}} - \Gamma_R n_{\text{qp}}^2 + \gamma_i - \Gamma_v n_{\text{qp}} e^{-(x-x_v^i)^2/l_v^2} = 0. \qquad (1)$$

D is the quasiparticle diffusion constant, which varies with energy, $D(E) = D_n[1 - (\Delta/E)^2]^{1/2}$ [20], where D_n is the normal metal diffusion constant. We take $D_n = 60$ cm^2/s based on previous work on quasiparticle diffusion in Al [23]. $D(E)$ has the strongest variation for quasiparticles with energies just above the gap, Δ, while D varies by only

~15% for energies above 2Δ. Because the pair-breaking radiation in our system is likely originating from the 3 K shield and warmer portions of our cryostat, the dominant part of this spectrum will lead to the majority of the nonequilibrium quasiparticles with energies of a few times Δ and above. Thus, to simplify the analysis while still capturing the essential dynamics, we take $D = D(2\Delta)$. We have explored the effects of varying D in our simulations and found that we can obtain reasonable agreement with our measurements over a wide range of D for physically realistic values of the other parameters in the simulations (see Supplemental Material [11], which includes Refs. [24,25]).

Γ_R is the effective background quasiparticle recombination rate in the Al film and is independent of position. The exact value of Γ_R depends on details of phonon trapping and is difficult to obtain precisely. Based on values extracted by others for Al thin films, Γ_R can be constrained to 10–100 $\mu m^3/s$ [20]. γ_i is the quasiparticle generation rate, which we also take to be independent of position, and we adjust the value of γ_i in order to match the value of n_{qp} with no vortices present that we obtain from our measured $1/Q_i$ for zero-field cooling.

The final term in Eq. (1) represents the quasiparticle-vortex interaction for one vortex centered at x_v^i. Γ_v corresponds to the rate of quasiparticle trapping and relaxation in the vicinity of the vortex, and thus this term has a strong spatial variation representing the suppression of the gap near the vortex core. We take the spatial dependence to be a Gaussian with a characteristic length scale $l_v = 0.5$ μm based on a treatment in Ref. [21] of the gap suppression near a vortex using the Usadel equations with a prediction of an effective radius of $\sim 2.7\xi$. Changing the functional form for this spatial variation or the value of l_v could impact the value of Γ_v that we extract, but the qualitative outcome would be unchanged.

We solve Eq. (1) with MATLAB by using a numerical package involving piecewise Chebyshev polynomial interpolants [26]. A damped Newton method is applied iteratively with an adaptive mesh to deal with the micron-scale features in the vicinity of each vortex while solving the nonlinear differential equation over the entire length L of the resonator. Because the open-ended geometry of our resonator avoids quasiparticle outdiffusion, we apply the boundary condition $\partial n_{qp}/\partial x = 0$ at both ends.

We simulate the field dependence of $n_{qp}(x)$ by including one vortex term for each vortex in the distribution for a particular field range. From the analysis of the steps in $1/Q_v$ for the fundamental, we extract the number of trapped vortices for each field range and then assign x_v^i for each of these to space them evenly in the middle 50 μm along x, corresponding to the central bulge region. We have checked that variations in the exact vortex positions in the bulge region have a negligible impact on our results (Supplemental Material [11]). At a cooling field of 72 μT, following the addition of the sixth vortex to the central bulge, there is a more rapid decrease in $1/Q_v$ for the harmonic (Fig. 3). This corresponds to the intermediate $B_{th}(6\ \mu m)$ for the 6-μm-wide coupling elbow, which is also at a current node. $B_{th}(6\ \mu m)$ is in between $B_{th}(8\ \mu m)$ for the bulge and $B_{th}(3\ \mu m)$ for much of the rest of the resonator. Because the area of the elbow region is about 3 times larger than that of the central bulge, beyond 72 μT we add one vortex to the elbow, evenly spaced within the elbow, every 1.7 μT while continuing to add one vortex to the bulge region every 5 μT.

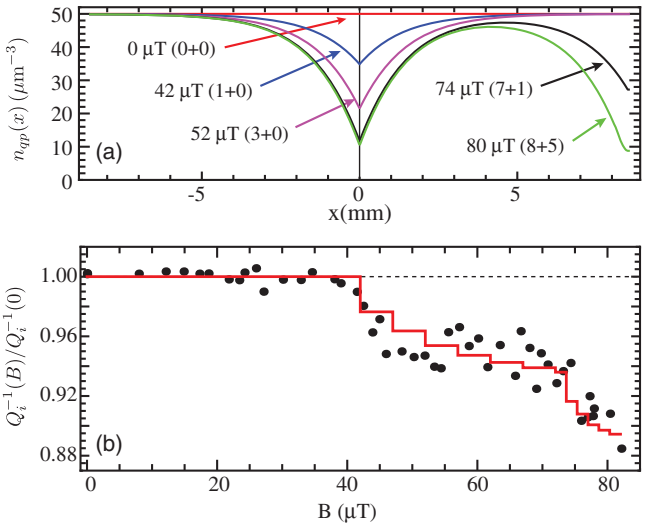

FIG. 4 (color online). (a) Simulated $n_{qp}(x)$ for several example fields. Labels indicate the vortex number in bulge + elbow. (b) Measured $1/Q_i(B)$ for the harmonic, normalized by the average of $1/Q_i$ below the threshold field (points); normalized quasiparticle loss on the harmonic from simulated $n_{qp}(x)$ (solid line).

Figure 4 contains several resulting $n_{qp}(x)$ profiles for four different vortex configurations. In order to compare the simulation results with the measured internal loss on the harmonic $1/Q_i(B)$, we account for the variation of the standing-wave current along the length of the resonator as described in the Supplemental Material [11]. We then compare this with the measured $1/Q_i(B)$ for the harmonic, normalized by the average of $1/Q_i(B)$ for $B < B_{th}(8\ \mu m)$. We then adjust Γ_v for the closest agreement between the simulations and the data. We have found that $\Gamma_R = 30\ \mu m^3/s$, consistent with earlier work for Al films [20], combined with $\Gamma_v = 3.5 \times 10^6\ s^{-1}$ provides a good match with the experiment [Fig. 4(b)], although for different D values there are moderately different values of Γ_R and Γ_v that also provide reasonable agreement with our data (Supplemental Material [11]). The value of Γ_v that we extract is in the range of typical electron-phonon scattering rates for Al thin films at low temperatures [27,28], although it is possible that electron-electron scattering in the vicinity of the vortex core may play a role as well [20].

While our simulations of n_{qp} provide a reasonable qualitative description of our loss measurements on the harmonic, they do not provide a perfect match to the data. For example, the initial decrease in $1/Q_i$ with the first few trapped vortices is not as rapid in our simulations compared to the experiment. In the future, a more sophisticated treatment of the quasiparticle diffusion and interaction with vortices could yield even better agreement and may reveal new features of this interaction.

Future devices could employ patterned pinning sites [5] in the trapping region to control the vortex location for further investigations of vortex dynamics and quasiparticle-vortex interactions. The ability to trap vortices in specific regions may be useful in hybrid superconducting-atomic systems as well [29].

We acknowledge useful discussions with J. M. Martinis, R. McDermott, and C. M. Wilson. During the preparation of this work, we became aware of related experiments on vortex trapping in superconducting qubits and a similar reduction in quasiparticle density [30,31], and we benefited from useful discussions with the authors of these works as well. This work was supported by the National Science Foundation under Grant No. DMR-1105197. Device fabrication was performed at the Cornell NanoScale Facility, a member of the National Nanotechnology Infrastructure Network, which is supported by the National Science Foundation (Grant No. ECCS-0335765).

*bplourde@syr.edu

[1] J. Clarke and F. K. Wilhelm, Nature (London) **453**, 1031 (2008).
[2] A. Wallraff, D. I. Schuster, A. Blais, L. Frunzio, R.-S. Huang, J. Majer, S. Kumar, S. M. Girvin, and R. J. Schoelkopf, Nature (London) **431**, 162 (2004).
[3] P. K. Day, H. G. LeDuc, B. A. Mazin, A. Vayonakis, and J. Zmuidzinas, Nature (London) **425**, 817 (2003).
[4] C. Song, T. W. Heitmann, M. P. DeFeo, K. Yu, R. McDermott, M. Neeley, J. M. Martinis, and B. L. T. Plourde, Phys. Rev. B **79**, 174512 (2009).
[5] C. Song, M. DeFeo, K. Yu, and B. L. T. Plourde, Appl. Phys. Lett. **95**, 232501 (2009).
[6] D. Bothner, T. Gaber, M. Kemmler, D. Koelle, and R. Kleiner, Appl. Phys. Lett. **98**, 102504 (2011).
[7] D. Bothner *et al.*, Appl. Phys. Lett. **100**, 012601 (2012).
[8] J. R. Clem, Bull. Am. Phys. Soc. **43**, 411 (1998).
[9] K. K. Likharev, Sov. Radiophys. **14**, 722 (1972).
[10] G. Stan, S. B. Field, and J. M. Martinis, Phys. Rev. Lett. **92**, 097003 (2004).
[11] See Supplemental Material at http://link.aps.org/supplemental/10.1103/PhysRevLett.113.117002 for further details of experimental setup, data analysis, and simulations.
[12] A. Megrant *et al.*, Appl. Phys. Lett. **100**, 113510 (2012).
[13] J. M. Martinis *et al.*, Phys. Rev. Lett. **95**, 210503 (2005).
[14] E. Bronson, M. P. Gelfand, and S. B. Field, Phys. Rev. B **73**, 144501 (2006).
[15] J. Healey, T. Lindström, M. Colclough, C. Muirhead, and A. Y. Tzalenchuk, Appl. Phys. Lett. **93**, 043513 (2008).
[16] R. Barends *et al.*, Appl. Phys. Lett. **99**, 113507 (2011).
[17] A. D. Corcoles, J. M. Chow, J. M. Gambetta, C. Rigetti, J. Rozen, G. A. Keefe, M. B. Rothwell, M. B. Ketchen, and M. Steffen, Appl. Phys. Lett. **99**, 181906 (2011).
[18] P. J. de Visser, J. J. A. Baselmans, P. Diener, S. J. C. Yates, A. Endo, and T. M. Klapwijk, Phys. Rev. Lett. **106**, 167004 (2011).
[19] J. M. Martinis, M. Ansmann, and J. Aumentado, Phys. Rev. Lett. **103**, 097002 (2009).
[20] J. N. Ullom, P. A. Fisher, and M. Nahum, Appl. Phys. Lett. **73**, 2494 (1998).
[21] A. Golubov and E. Houwman, Physica (Amsterdam) **205C**, 147 (1993).
[22] J. T. Peltonen, J. T. Muhonen, M. Meschke, N. B. Kopnin, and J. P. Pekola, Phys. Rev. B **84**, 220502 (2011).
[23] S. Friedrich, K. Segall, M. Gaidis, C. Wilson, D. Prober, A. Szymkowiak, and S. Moseley, Appl. Phys. Lett. **71**, 3901 (1997).
[24] A. Anthore, H. Pothier, and D. Esteve, Phys. Rev. Lett. **90**, 127001 (2003).
[25] J. Pekola, D. Anghel, T. Suppula, J. Suoknuuti, A. Manninen, and M. Manninen, Appl. Phys. Lett. **76**, 2782 (2000).
[26] L. N. Trefethen *et al.*, CHEBFUN version 4.2, 2011, http://www.chebfun.org.
[27] S. B. Kaplan, C. C. Chi, D. N. Langenberg, J. J. Chang, S. Jafarey, and D. J. Scalapino, Phys. Rev. B **14**, 4854 (1976).
[28] C. C. Chi and J. Clarke, Phys. Rev. B **19**, 4495 (1979).
[29] O. Romero-Isart, C. Navau, A. Sanchez, P. Zoller, and J. I. Cirac, Phys. Rev. Lett. **111**, 145304 (2013).
[30] C. Wang *et al.*, arXiv:1406.7300.
[31] U. Vool *et al.*, arXiv:1406.1769.